Influence of annealing temperature of α- Fe_2O_3 nanoparticles on Structure and Optical Properties.

Eman. K Tawfik[1],[*], Wael H.Eisa[2], N. Okasha[3], H.A.ashry[1].

[1]Radiation Physics Department, National Centre for Radiation Research and Technology(NCRT), Atomic Energy Authority (AEA), Nasr City, Cairo, Egypt.

[2]Spectroscopy Department, Physics Division, National Research Centre (NRC), Egypt.

[3]Physics Department, Faculty of Women, Ain Shams University, Cairo, Egypt.

Abstract

This work has been focused on the synthesis of the raw materials iron oxide nanoparticles; hematite (α -Fe_2O_3) from Iron (II) chloride tetra hydrate ($FeCl_2$-$4H_2O$) and iron (III) chloride hexahydrate ($FeCl_3$-$6H_2O$) using Solid State Chemical Reaction technique. Nanostructure powders were characterized by X-ray diffraction (XRD), scanning electron microscope (SEM), energy dispersive X-ray spectroscopy (EDX), and UV-visible spectroscopy. XRD confirmed the formation of crystalline α -Fe_2O_3 nanostructured and its average crystallite size increased from ~ 12 to 28 nm with increasing annealing temperature from 200 up to 80℃ while SEM confirmed the morphology and the purity of the sample was evaluated from the energy dispersive spectrum (EDS). Moreover, strain decreased with increasing annealing temperature. UV-visible characterization indicated the existence of both direct and indirect band gap in the samples. All The annealed samples showed the direct band gap at ~ 2.21 eV. However, the indirect band gap increased from 1.6 to 1.94 eV when the annealing temperature increased from 200 up to 700℃ and remained almost the same for sample annealed at 800℃. The observed values of optical band gaps were in close agreement with the reported values. Our results indicated that the annealing would give rise to a good crystalline α -Fe_2O_3 nanoparticles with reduced strain.

Keywords: *Hematite; XRD; EDS; SEM; Strain; Optical properties.*

1. Introduction

In recent years, research on transition metal oxide (TMOs) nanoparticles has attracted much attention for their potential technological applications. Iron oxide is one of the most important transition metal oxides. Iron oxide exhibits different phases such as FeO, α-Fe_2O_3, γ -Fe_2O_3,β-Fe_2O_3 and Fe_3O_4. Hematite (α-Fe_2O_3) is the most stable iron oxide under ambient conditions. It is a low cost non-toxic environment friendly material easily available in nature [2] .

***Corresponding author**: Eman. K Tawfik**,** [1]Radiation Physics Department, National Centre for Radiation Research and Technology(NCRT), Atomic Energy Authority (AEA), Nasr City, Cairo, Egypt.

E- mail:Eman_tawfik10@yahoo.com

It shows n-type semiconducting properties with band gap = 2.2eV which lies in the visible region [3]. α-Fe_2O_3 exhibits rhombohedral centered hexagonal structure of the corundum type with a close packed oxygen lattice in which two-thirds of the octahedral sited are occupied by Fe (III) ions [4]. α -Fe_2O_3 shows canted antiferromagnetic (weakly ferromagnetic) at room temperature, antiferromagnetic below the Morin transition temperature of 250 K and paramagnetic above its Néel temperature of 948 K [5]. α -Fe_2O_3 displays wide ranges of applications such as light-induced water splitting [6] , catalysis[7], gas sensors [8], solar cells[9], field emission devices[10], magnetic recording [11], drug delivery [12], tissue repair engineering [13], magnetic resonance imaging [14], pigments [15], lithium-ion batteries [11] and spin electronic devices[16].

Several methods have been adopted for the synthesis of nanoparticles of α-Fe_2O_3 such as sol–gel [17], chemical precipitation [18], forced hydrolysis [19,20], hydrothermal [21, 22], sonochemical [23], solution combustion [24], high-energy ball milling [25] etc. Among the above methods, some of them are very expensive and requisite large time for the synthesis of final product. It is therefore necessary that the synthesis route would facilitate for large scale synthesis of nanoparticles of α-Fe_2O_3 in cost effective and easier method.

The aim of this work was the synthesis of α-Fe_2O_3 nanoparticles via solid state chemical reaction and studied the effect of annealing temperature on their structure as size and shape, microstructure, and optical properties. As well as an interesting anode material this has been investigated for a wide range of applications. It has found application in the manufacturing of gas sensors, catalysis, magnetism, lithium ion batteries and electrochemical capacitors.

2. Materials and Method

Materials

Iron (II) chloride tetrahydrate ($FeCl_2.4H_2O$), iron (III) chloride hexahydrate ($FeCl_3.6H_2O$), Poly vinyl pyrrolidone (PVP), and potassium chloride, were purchased from LOBA CHEMIE, India and all reagents were of analytical grade and synthesized without further purification. All solutions were prepared using de-ionized water.

Preparation of Iron Oxide Nanoparticles by Solid State Chemical Reaction technique

For the synthesis of iron oxide nanoparticles as solid phase, all the powders of $FeCl_3.6H_2O$ (1.35 g), $FeCl_2.4H_2O$ (0.50 g), KCl (3.9 g), and PVP (1g) were mixed and ground in agate mortar for 30 min at room temperature . The resulted mixture from grinding was a yellow paste. KOH powder (1.22 g) was added, followed by grinding for another 30 min at room temperature. During the KOH addition and the subsequent grinding, a significant amount of heat and some vapor was given off in the first few minutes. The product was washed several times with the distilled water then ethanol, treated in an ultrasonic bath for 15 min and centrifuged (3,500 rpm) for 10 min. This process was repeated several times until no Cl^- ion could be detected in the centrifuge. The product was then dried at 50 ºC which became brown as nano-powder. Drying samples were ground and annealed at different temperature (200,300,400,500,600,700, and 800)°C. The samples were allowed to cool down to room temperature then the obtained powder kept in desiccator oven silica gel. The hematite (α-Fe_2O_3) nanoparticles are formed.

Characterization techniques

The crystal structures were studied by a powder X-ray diffractometer (shimadzu XRD 6000) prepared with Cu Kα as radiation source (λ = 1.54Å.) in the 2θ range 15 to 80° with step size of 0.025°.The XRD Patterns of nanoparticles were confirmed by comparing with the ICDD card. The morphology and chemical composition of the synthesized iron oxide nanoparticles were observed by scanning electron microscopy/energy dispersive X-ray analysis (SEM/ EDAX, Philips XL-30). The static magnetic properties for the samples in the powder were carried out at room temperature using a Model 4HF vibrating sample magnetometer with a maximum magnetic field of 20 kOe. The UV–vis spectra measurements were recorded using V-630 UV-Vis spectrophotometer (Jasco, Japan).

3. Results and discussion

3.1. Characterization of the (α-Fe_2O_3 NPS)

3.1. a. X-ray diffraction (XRD) characterization of the α-Fe_2O_3 .

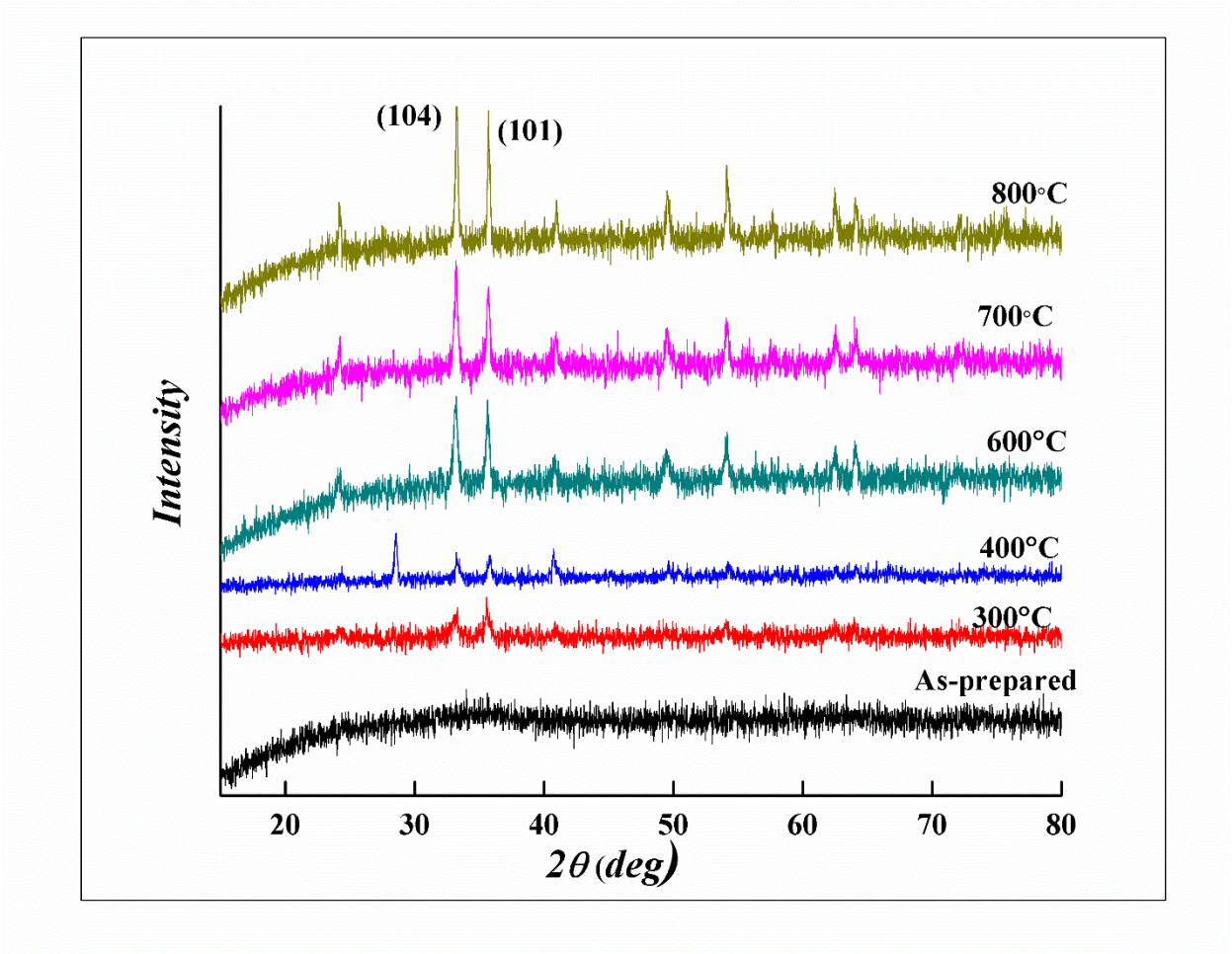

Fig. 1: XRD pattern of α-Fe_2O_3 nanoparticle as prepared and annealed at different temperatures.

The composition and crystalline phase purity of the as-prepared and annealed products were examined by XRD. Fe_2O_3 exhibits two well-known crystalline phases: γ-Fe_2O_3 (maghemite) with cubic structure and α-Fe_2O_3 (hematite) with rhombohedral structure [26] . Fig.1 shows the XRD patterns of the as-prepared and annealed Fe_2O_3 samples. It is clear that, XRD pattern of the as-prepared sample did not show any diffraction peaks and low intensity broad to be detected indicating it is amorphous. This might be due to the small grain size and/or low degree of crystallinity of the as-prepared samples.

After annealing treatment at 300, 400, 600, 700, and 800 ^{o}C, the XRD pattern of the amorphous phase crystallizes into the more stable polymorph α-Fe_2O_3 with increasing temperature. The diffraction peaks appeared at 2θ = 24.16^{o}, 33.11^{o}, 35.62^{o}, 40.86^{o}, 49.46^{o}, 54.11^{o}, 62.34^{o}, 64.02^{o}, and71.89^{o} are assigned to the planes (012), (104), (110), (113), (024), (116), (214), (300), and (101) respectively. This diffraction pattern can be indexed to the rhombohedral phase of α-Fe_2O_3 (ICDD card no. 33-0664). It has been reported that the annealing treatment gives rise to the crystallization into the more stable polymorph α-Fe_2O_3 at about 400^{o}C [1, 27].

The sample annealed at 300^{o}C shows a low intensity peaks, indicating the existence of defects and low crystallization degree. As the temperature increases from 300 to 800^{o}C, XRD peaks intensity of α-Fe_2O_3 increases and the FWHM decreases, suggesting a growing of crystal domain size [28].

On careful analysis of the XRD patterns, it is found that the (104) and (110) are more pronounced than the other peaks. The plane (104) is related to the near basal plane (a-axis), whereas the plane (110) is related to the no basal plane (c-axis). As the FWHM of the 104 line decreases, the crystal is more elongated along the c-axis. Also, in the narrower 110 plane, the crystal is longer (thicker) in the a-axis direction [29] indicated that, the crystallite size relates to the crystallite dimensions along the c-axis direction. (110) Bragg reflections is dominated for sample annealed at 300^{o}C indicating that the crystalline phase of α-Fe_2O_3 is preferentially oriented along the [110] direction. As the annealing temperature is gradually increased from 300 up to 800^{o}C (all other parameters are kept unchanged), (104) peak increases with the simultaneous decrease of the (110) peak. This suggests that [104] direction is the preferential orientation of α-Fe_2O_3 at high annealing temperatures. The values of the intensity and FWHM of planes (104) and (110) are given in **Table 1**. It can be seen that the FWHM of planes (104) and (110) decreases to 54% and 67% as the annealing temperature increases from 300 to 800^{o}C. Hence, the particles tend to be thicker and larger.

Table 1: The values of FWHM for (104) and (110) XRD peaks of hematite (α-Fe_2O_3).

Annealing Temperature (°C)	Intensity%			FWHM		
	(104)	(110)	$I_{(104)}/I_{(110)}$	(104)	(110)	$FWHM_{(104)}/FWHM_{(110)}$
300	75.99	91.58	0.45	0.59	0.45	1.31
400	90.38	81.83	0.52	0.50	0.33	1.51
600	232.55	191.64	0.55	0.43	0.38	1.11
700	251	208.72	0.55	0.38	0.36	1.07
800	329.2	241.12	0.58	0.32	0.30	1.06

3.1. b. Effect of annealing temperature on the microstructural properties

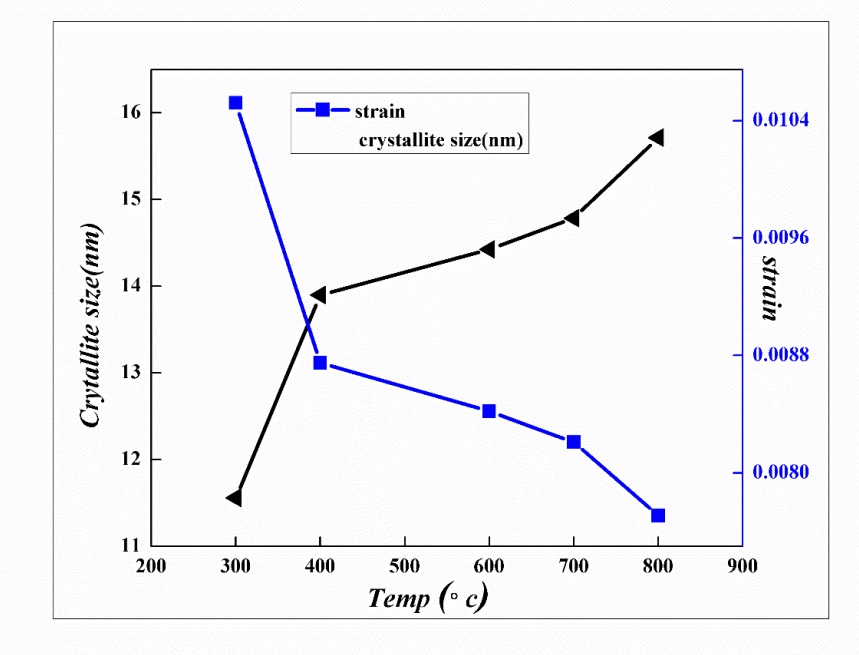

Fig. 2: Variation of crystallite size and strain for α-Fe_2O_3 nanoparticle annealed at different temperature.

In order to study the effect of annealing temperature on the microstructural properties we estimated the average crystallite size (D) and the strain (ε) present in α-Fe_2O_3nanoparticles from the full width at half maximum (FWHM) of the first major XRD peak using the following Debye Scherer equations [30] :

$$D = \frac{K\lambda}{\beta COS\theta} \quad (1)$$

$$\varepsilon = \frac{\beta}{4tan\theta} \quad (2)$$

Where β is the FWHM, θ is the Bragg's angle and λ is the wavelength of Cu Kα radiation. Fig. 2 shows the variation of crystallite size and strain for α-Fe_2O_3 nanoparticle annealed at different temperatures.

It is revealed from the figure that, crystallite size increased from ~ 12 to 28 nm when annealing temperature increased from 300 to 800ºC. So this means that, samples contain relatively smaller crystallites even though when use higher annealing temperature. Moreover its notes that, the strain for the same studied samples decreased with increasing annealing temperature. This behavior attributed the reflected in the optical band gap .According to [31] for extremely small size particles, surface pressure increases, hence lattice strain increases, which decreases the band gap. Our results indicated that with increasing the annealing temperature the particle size increase, surface pressure decrease hence lattice strain decrease .where the band gap in nanoparticles may be affected which related to three factors.

1. Surface and interface effect
2. Change in crystal structure by heat treatment
3. Lattice strain in the sample.

Our results indicated that the annealing is essential for synthesis of good crystalline strain free α-Fe_2O_3 nanoparticles.

3.2. UV–vis spectroscopy

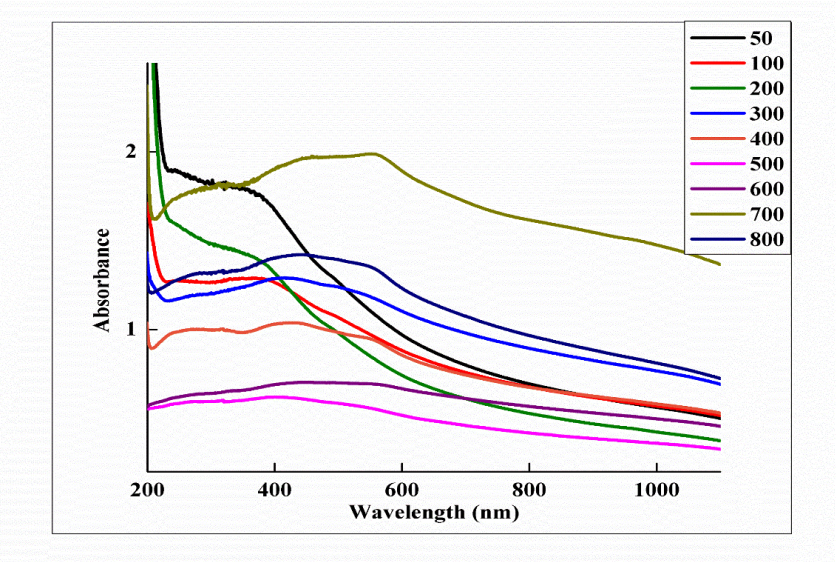

Fig .3: Variation of absorption coefficient of α -Fe_2O_3 nanoparticle at different annealing temperature with wavelength.

Figure (3) illustrate the absorption spectra of iron oxide nanoparticles at different temperatures (50,100,200,300,400,500,600,700, and800)˚C by using UV-Visible absorption spectroscopy. It is clear that, at high absorption visible region, the peak absorbance at around 400 nm indicated that, the edges bands of absorption spectra is located at between (400-600) nm The optical band gap has been calculated using Tupac's equations:

$$\alpha h\nu = A(h\nu - Eg)^n \quad (1)$$

where

$$\alpha = 2.303\left(\frac{A}{t}\right) \quad (2)$$

where **hν** is the photon energy, **α** is the absorption coefficient, **A** is constant relative to the material, **t** is the thickness of the sample (i.e 1cm for cuvette) , **n** is either 2 for direct transition or ½ for indirect transition. After substitution n=1/2 & n= 2 the Tauc formula will be as follows in Eq.3& 4 respectively, [32].

• For direct band gap:

$$(\alpha h\upsilon)^2 = A\left(h\nu - E_g\right) \quad (3)$$

• For Indirect band gap:

$$(\alpha h\upsilon)^{1/2} = A\left(h\nu - E_g\right) \quad (4)$$

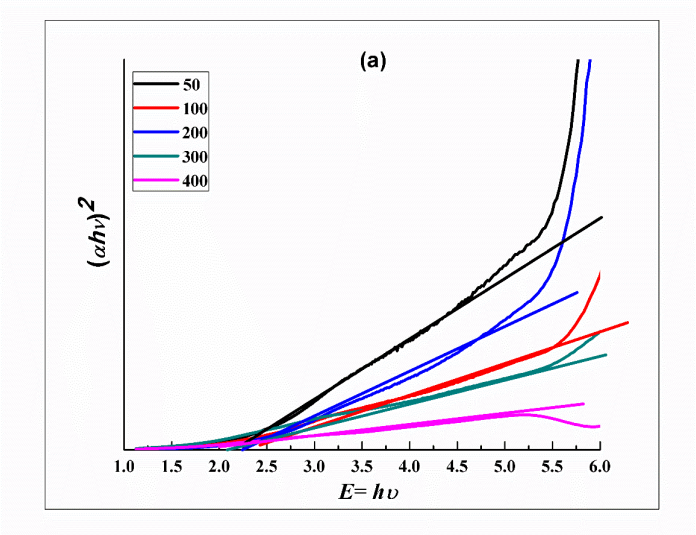

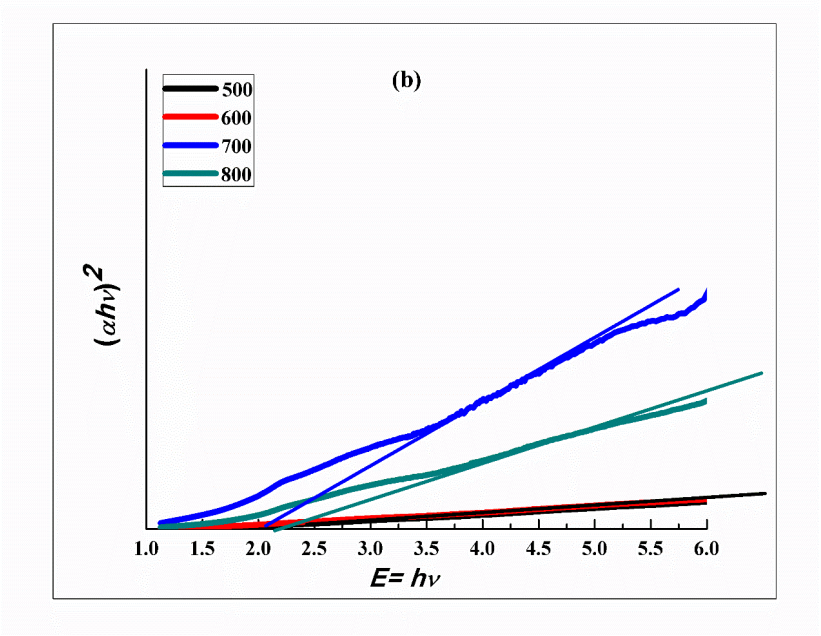

Fig.4: Variation of $(\alpha h\nu)^2$ vs. photon energy, hν for α -Fe_2O_3 nanoparticles annealed at different Temperatures (a) and (b).

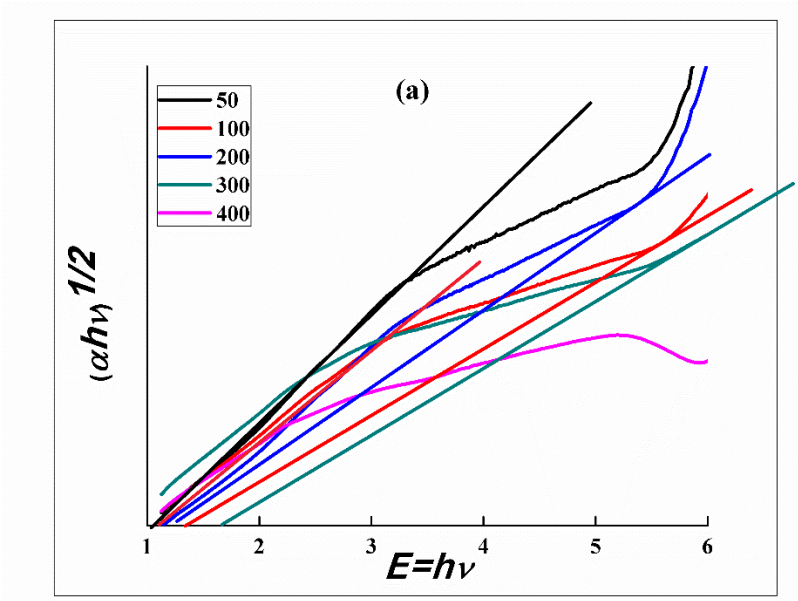

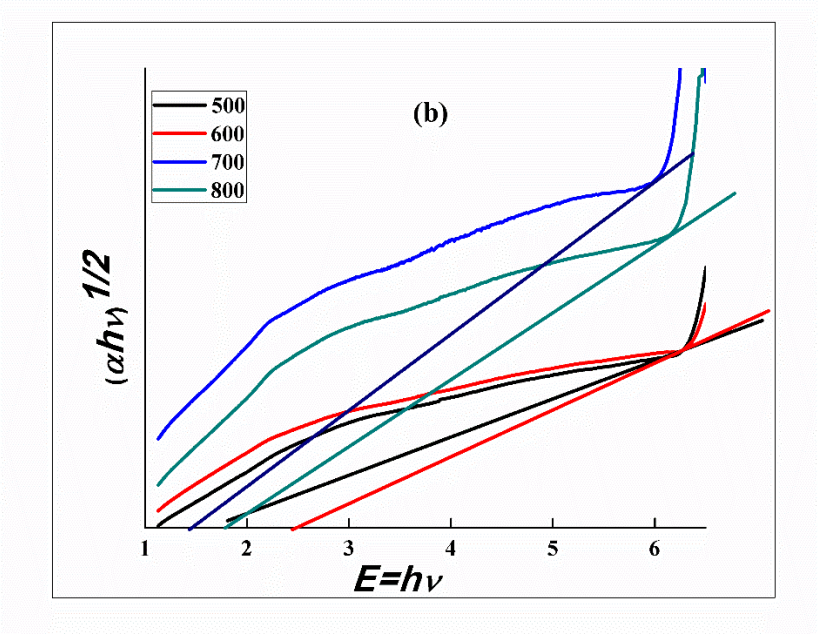

Fig.5: Variation of $(\alpha h\nu)^{1/2}$ vs. photon energy, hν for α -Fe_2O_3 nanoparticles annealed at different temperatures (a) and (b).

Some reports indicated that α-Fe_2O_3 is an indirect band gap material [33, 3] and some other reported the existence of direct band gap in α-Fe_2O_3 [34]. It has also been reported that α -Fe_2O_3 exhibits both direct band gap and indirect band gaps [35, 36]. The spin forbidden Fe^{3+} 3d→3d excitation gives rise to indirect transition and the direct transition corresponds to the O_2- 2p →Fe^{3+} 3d charge transfer [37].Hence the optical band gap for absorption peak can be achieved by the extrapolating the linear portion of the $(\alpha h\nu)^{n}$ – hν curve to zero. Fig(4) show The value of direct band gap of iron oxide nanoparticles decreased from ~3.3 eV for the pure α-Fe_2O_3 [2] to ~2.22 eV for the α-Fe_2O_3 nanoparticle with increasing temperatures, The reduction in direct band gap is due to increase in the grain size with increasing the temperature [38, 39]. Therefore, the blue shift in the band gaps with reduction in grain size is due to the quantum confinement effect [40]. Unlike direct band gap, Fig (5) show the indirect band gap increased from 1.1to 1.9 eV when the annealing temperature increased from 400 to 800℃, where the value of direct and indirect bandgap shown in table (2).

Table (2): Variation of direct and indirect band gap of α- Fe2O3 nanoparticle composites with different annealing temperature.

Sample	E_g direct (ev) $(\alpha h\nu)^2$ Vs.hν	E_g indirect (ev) $(\alpha h\nu)^{1/2}$ vs.hν
As prepared 50	3.33	1.1
100	3.33	1.1
200	3.33	1.1
300	3.23	1.2
400	2.72	1.4
500	2.62	1.5
600	2.42	1.6
700	2.3	1.8
800	2.22	1.9

3.3. SEM&EDX analysis

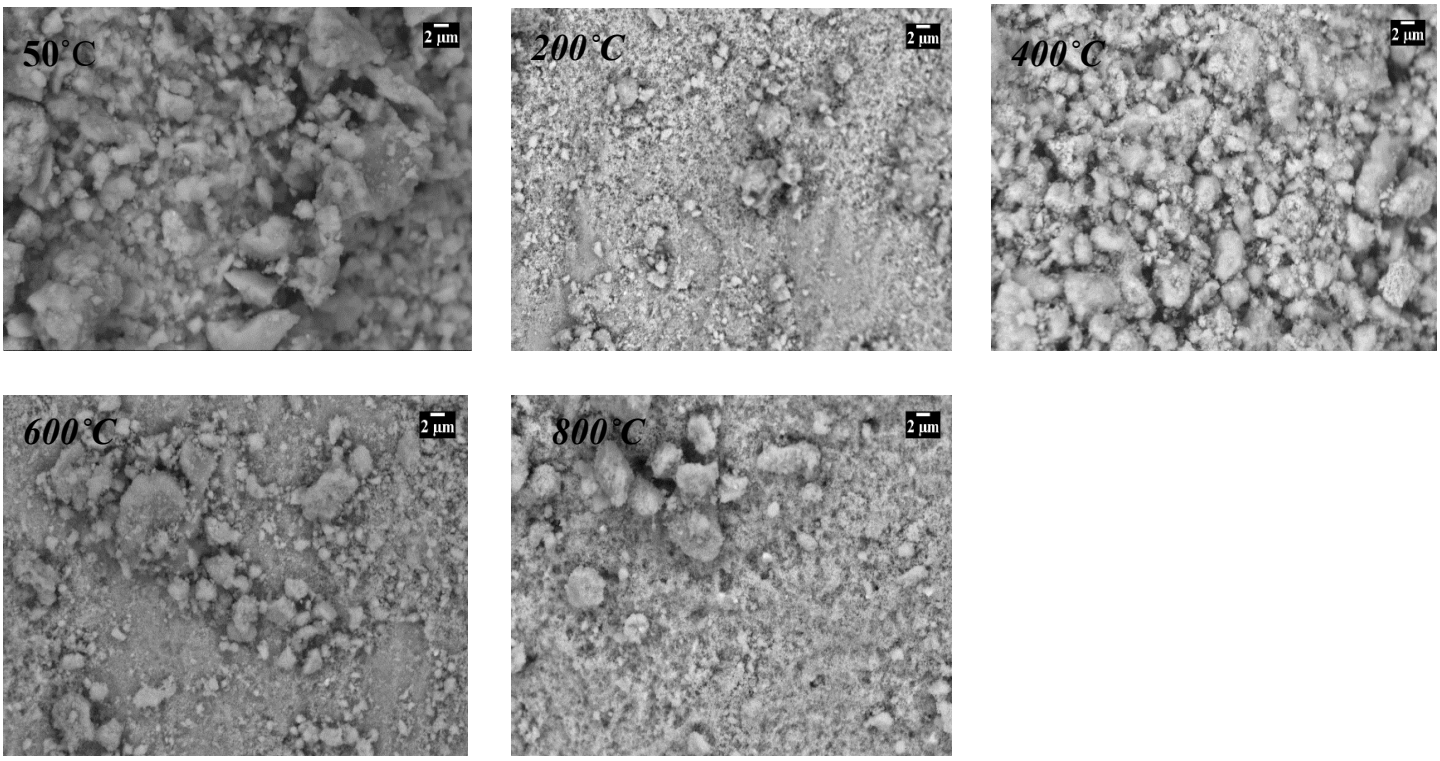

Fig. 6: SEM of the iron oxide nanoparticles of as- prepared and annealed at different temperature (200,400, 600 &800)ºC for 2 h.

Figure 6 showed that, SEM images of the as-prepared sample and different annealing temperature of α-Fe_2O_3 nanoparticles. As the calcination temperature increased, the particles become finer and forming nearly spherical shaped particles. The average particle size calculated is 55 nm. The measured particle size using SEM measurements appears to be greater than that measured using XRD [41] [42]. This suggests that the observations made by electron microscopes give grain size or particle size that may be consisted of more than one crystallite, while the XRD gives the crystallite size.

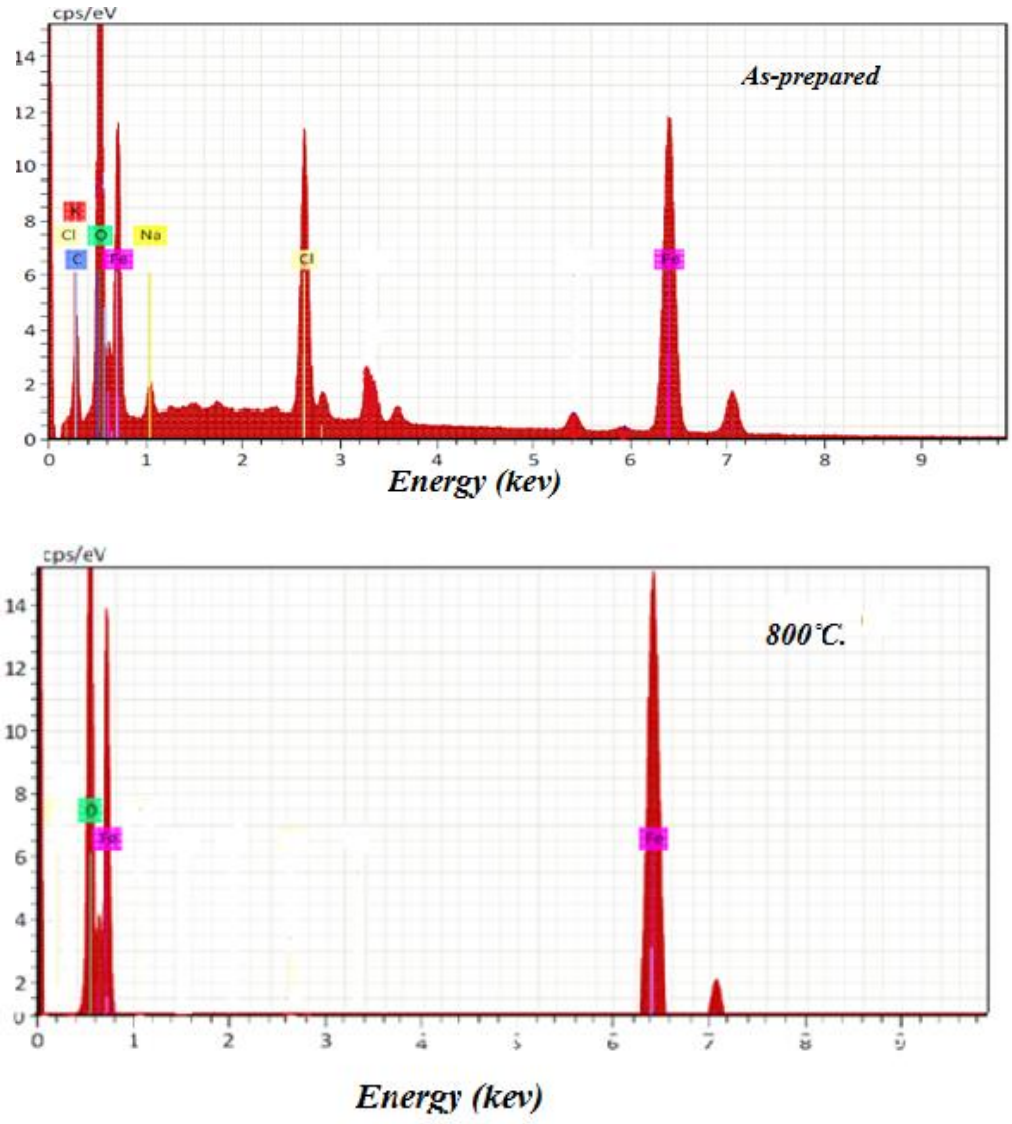

Figure 7: EDAX spectra of synthesized iron oxide nanoparticles of as-prepared sample and at 800˚C.

The composition of the prepared α-Fe_2O_3 nanoparticles is confirmed by observing the EDAX Spectrum. The EDAX spectra for the α-Fe_2O_3 nanoparticles are given in the Fig. 7. α-Fe_2O_3 nanoparticle calcined at 800°C has the peaks of iron and oxygen alone. The other samples have some impurities which are removed as the calcination temperature increases.

3.4. Magnetic properties:

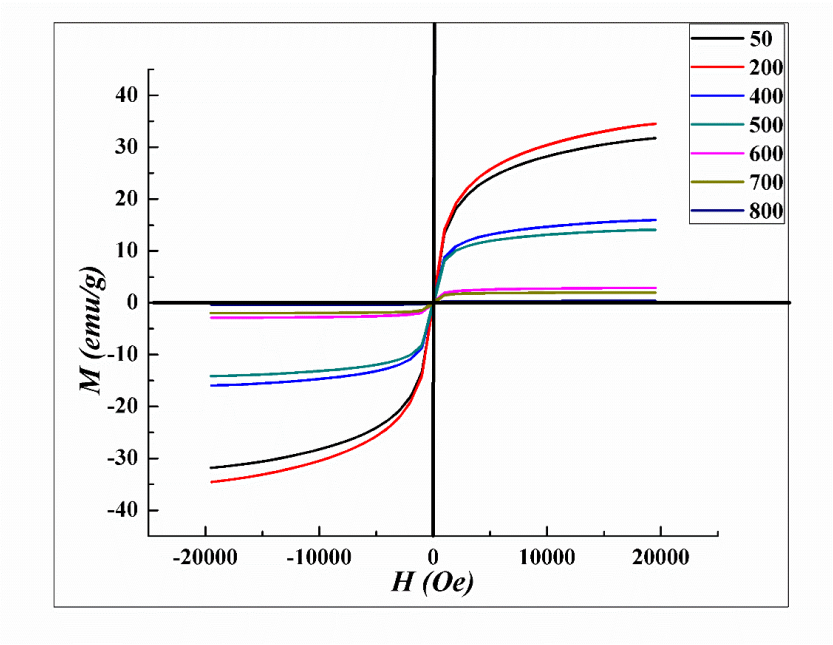

Fig.8: Room temperature magnetization curves of the synthesized hematite nanoparticles with different annealing temperature.

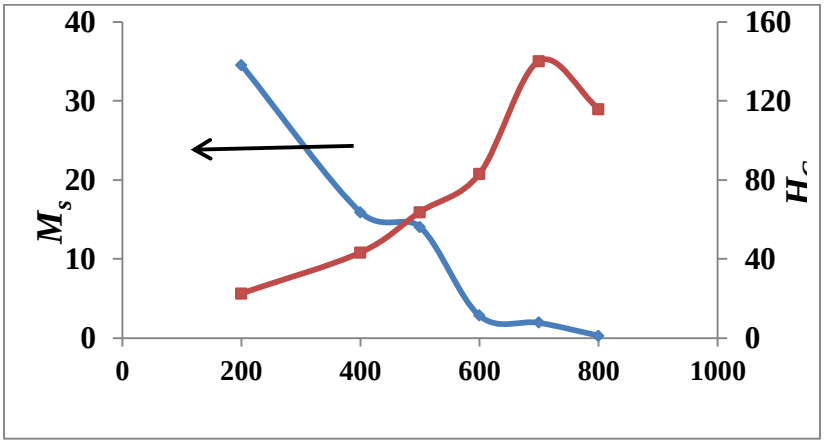

Fig.9: The effect of annealing temperature on the saturation magnetization (M_s) and the coercivity (H_C).

Figure (8) shows the magnetic hysteresis loops of the α-Fe_2O_3 nano-structures obtained at different temperature (50,200,400,500,600,700,800). It can be seen that the nanostructures all exhibit weak ferromagnetic behaviors and the curves obtained of magnetization versus magnetic field do not show any saturation even up to the maximum applied magnetic field of 20 kOe. The complete values of the saturation magnetization ($\mathbf{M}_s$) and coercivity (H_c) of the as- prepared α-Fe_2O_3 samples at different temperatures are summarized in Table 3. It is easy to find that the magnetization of the nano-particle samples is decreased with temperature but coercivity force of the samples increase with temperature of the nanoparticles. It is well-known that the magnetization of ferromagnetic materials is very sensitive to the morphologies and structures of the as-prepared samples and this is agree well with [43].

Table (3): The value of the magnetization (Ms) and coercivity (Hc) of the as-prepared samples.

Samples	Saturation Magnetization (M_S) emu/g	Coercivity (H_c) G	Remanent magnetization (Mr) emu/g
50	31.787	28.889	0.40275
200	34.550	22.7344	0.32810
400	15.953	43.399	0.39512
500	14.111	63.910	0.56964
600	2.8810	83.155	0.17282
700	0.37040	140.13	0.24286
800	1.9951	115.92	33.727E-3

But the typical static magnetic parameters including coercivity (H_C) and remanent magnetization (M_r) etc. are remarkably different with the samples obtained at different T as in Fig (9). Among these samples obtained at (50, 200, 300, 500, 600, 700 and 800ºC) the samples formed at 400ºC shows a typical multidomains type behavior and have the best soft magnetic properties with the highest saturation magnetization (M_s) of more than 1.995 emu.g^{-1}, the lowest M_r, H_C, and squareness (M_r/M_s) of 0.40275 emu g^{-1}, 28.889 Oe, and 0.01267, respectively. The samples formed at 800ºC have the largest M_r (33.727e10^{-3} emu g^{-1}) and H_c (115.92 Oe). It is worth mentioning that the coercivity and squareness of the samples formed at 800ºC are both one order of magnitude higher than those of the samples obtained at 100ºC and 400ºC. Meanwhile, they are also significantly higher than those of polycrystalline α-Fe_2O_3 nanostructures synthesized by a

hydrothermal synthetic route (Zhu et al. 2006), α-Fe_2O_3 rhombohedra nanoparticles (Jing and Wu 2004). The magnetization of ferromagnetic materials was believed to be highly dependent on the geometry morphology, size, and crystallization of the materials. The different magnetic properties of the α-Fe_2O_3 complex nanostructure obtained at different Temp may be attributed to the combined effects of the morphology, crystal size, and crystal structures. The high M_r and H_C of the sample obtained at 800ºC may be attributed to the magneto static dipole interactions and/or the shape anisotropy in the high-crystalline complex nanostructures in this work.

Conclusion

- An environmentally benign method was developed to fabricate iron oxide (α-phase nanoparticles α-Fe_2O_3 .
- XRD spectra were recorded to confirm the evolution of single phase α-Fe_2O_3 .SEM, EDAX, VSM and UV-Vis spectroscopic studies on the prepared α-Fe_2O_3 nanoparticles reveal the successful synthesis and characterization of hematite nanoparticles.
- The crystallite size of hematite nanoparticles ranged from 12 to 28.
- Magnetic performances of the Fe_2O_3 products are illustrated; meanwhile the as-prepared single crystal nanoparticles show a significant enhancement of coercivity.

Acknowledgement

The present work was supported by the research funds of cooperation between National Center for Radiation Research and Technology (NCRRT), National Research Center (NRC) & Girls collage for Arts, Sci. and Ed. Ain Shams University, Cairo, Egypt. The authors would like to thank for their support.

References

[1] T.M. McCoy, P. Brown, J. Eastoe, R.F. Tabor, "Noncovalent magnetic control and reversible recovery of graphene oxide using iron oxide and magnetic surfactants", ACS Appl. Mater. Interfaces. **7** (2015) 2124–2133. doi:10.1021/am508565d.

[2] P. Mallick, B.N. Dash, "X-ray Diffraction and UV-Visible Characterizations of α-Fe_2O_3 Nanoparticles Annealed at Different Temperature", Nanosci. Nanotechnol. **3** (2013) 130–134. doi:10.5923/j.nn.20130305.04.

[3] M.F. Al-Kuhaili, M. Saleem, S.M.A. Durrani, "Optical properties of iron oxide (α-Fe_2O_3)

thin films deposited by the reactive evaporation of iron", J. Alloys Compd. **521** (2012) 178–182. doi:10.1016/j.jallcom.2012.01.115.

[4] M. Properties, S. "Characterization, Iron (III) Oxides from Thermal Processes Synthesis" , (2002) 969–982.

[5] L. Canilha, A.K. Chandel, T. Suzane, F. Antunes, W. Luiz, M. Grac, A. Felipe, S. Silv, Bioconversion of Sugarcane Biomass into Ethanol : An Overview about Composition , Pretreatment Methods , Detoxification of Hydrolysates , Enzymatic Saccharification , and Ethanol Fermentation, 2012 (2012). doi:10.1155/2012/989572.

[6] Catherine M. Aitchison , Reiner Sebastian Sprick , Andrew I. Cooper ,"Emulsion polymerization derived organic photocatalysts for improved light-driven hydrogen evolution" ,11- 013, 128 (2007) 15721.

[7] T. Ohmori, H. Takahashi, H. Mametsuka, E. Suzuki, "Photocatalytic oxygen evolution on a -Fe O Đlms using Fe^3 ‘ ion as a sacriÐcial oxidizing agent, (2000) 3519–3522.

[8] X. Gou, G. Wang, J. Park, H. Liu, J. Yang, "Monodisperse hematite porous nanospheres: Synthesis, characterization, and applications for gas sensors", Nanotechnology. 19 (2008). doi:10.1088/0957-4484/19/12/125606.

[9] H. Zhou, S.S. Wong, A Facile and Mild Synthesis of 1-D ZnO , 2 (n.d.).

[10] D. Zitoun, N. Pinna, N. Frolet, C. Belin, L. Agre, "Single Crystal Manganese Oxide Multipods by Oriented Attachment", (2005) 15034–15035.

[11] C. Wu, P. Yin, X. Zhu, C. Ouyang, Y. Xie, "Synthesis of Hematite (r -Fe_2O_3) Nanorods : Diameter-Size and Shape Effects on Their Applications in Magnetism , Lithium Ion Battery , and Gas Sensors", (2006) 17806–17812. doi:10.1021/jp0633906.

[12] K.J. Widder, A.E. Senyei, D.G. Scarpelli, D.G. Scarpelli, Experimental Biology and Medicine, (1978). doi:10.3181/00379727-158-40158.

[13] G. Garçon, S. Garry, P. Gosset, F. Zerimech, A. Martin, M.H. Hannothiaux, P. Shirali, Benzo(a)pyrene-coated onto Fe2O3 particles-induced lung tissue injury: Role of free radicals, Cancer Lett. 167 (2001) 7–15. doi:10.1016/S0304-3835(01) 00474-8.

[14] R. Lawaczeck, M. Menzel, H. Pietsch, Superparamagnetic iron oxide particles: Contrast media for magnetic resonance imaging, Appl. Organomet. Chem. **18** (2004) 506–513. doi:10.1002/aoc.753.

[15] D. Walter, Characterization of synthetic hydrous hematite pigments, Thermochim. Acta. **445** (2006) 195–199. doi:10.1016/j.tca.2005.08.011.

[16] M. Busch, M. Gruyters, H. Winter, Spin polarization and structure of thin iron oxide layers prepared by oxidation of Fe(110), Surf. Sci. **600** (2006) 4166–4169. doi:10.1016/j.susc.2006.01.140.

[17] M.H. Key, B. Edwards, E.C. Harvey, G.J. Hirst, C.J. Hooker, A.K. Kidd, E.M. Madraszek, P.A. Rodgers, I.N. Ross, M.J. Shaw, M. Steyer, the brightness, B, (W cm2 sr1) is B =, **1397** (1990) 9–17.

[18] A. Glisenti, C. Inorganica, M. Analitica, U.Ï. Padova, R. August, A. October, Interaction of formic acid with Fe O powders under di † erent atmospheres : an XPS and FTIR study, (1998).

[19] H. Search, C. Journals, A. Contact, M. Iopscience, S.S. Phys, I.P. Address, Size-induced structural phase transitions and hyperfine properties of microcrystalline Fe , O , 2229 (1988).

[20] K. Cheng, Y.P. He, Y.M. Miao, B.S. Zou, Y.G. Wang, T.H. Wang, Quantum Size Effect

on Surface Photovoltage Spectra : Alpha-Fe_2O_3 Nanocrystals on the Surface of Monodispersed Silica Microsphere, (2006) 7259–7264.

[21] S. Giri, S. Samanta, S. Maji, S. Ganguli, A. Bhaumik, Magnetic properties of a -Fe_2O_3 nanoparticle synthesized by a new hydrothermal method, 285 (2005) 296–302. doi:10.1016/j.jmmm.2004.08.007.

[22] J. Lian, X. Duan, J. Ma, P. Peng, T. Kim, W. Zheng, Hematite (α -Fe_2 O_3) with Various Morphologies: Ionic Liquid-Assisted Synthesis, Formation Mechanism, and Properties, 3 (2009) 3749–3761.

[23] P. Taylor, A. Askarinejad, M. Bagherzadeh, A. Morsali, Sonochemical fabrication and catalytic properties of α-Fe_2O_3 nanoparticles, (2011) 37–41. doi:10.1080/17458080.2010.489583.

[24] P. Sharma, S. Dhiman, S. Kumari, P. Rawat, C. Srivastava, Revisiting the physiochemical properties of Hematite (α-Fe_2O_3) nanoparticle and exploring its bio-environmental application Revisiting the physiochemical properties of Hematite (α -Fe_2O_3) nanoparticle and exploring its bio-environmental application, (2019).

[25] S. Yang, X. Song, P. Zhang, J. Sun, L. Gao, Self-Assembled α -Fe_2O_3 Mesocrystals / Graphene Nanohybrid for Enhanced Electrochemical Capacitors, (2014) 2270–2279. doi:10.1002/smll.201303922.

[26] G. Tong, J. Guan, Z. Xiao, X. Huang, Y. Guan, In situ generated gas bubble-assisted modulation of the morphologies, photocatalytic, and magnetic properties of ferric oxide nanostructures synthesized by thermal decomposition of iron nitrate, J. Nanoparticle Res. 12 (2010) 3025–3037. doi:10.1007/s11051-010-9897-2.

[27] L. Lu, L. Li, X. Wang, G. Li, Understanding of the finite size effects on lattice vibrations and electronic transitions of nano α-Fe2O3, J. Phys. Chem. B. 109 (2005) 17151–17156. doi:10.1021/jp052780+.

[28] Y. Lin, P.R. Abel, A. Heller, C.B. Mullins, α -Fe_2O_3 Nanorods as Anode Material for Lithium Ion Batteries, (2011) 2885–2891.

[29] M. Mohammadikish, Hydrothermal synthesis , characterization and optical properties of ellipsoid shape α -Fe_2 O_3 nanocrystals, Ceram. Int. (2013) 1–8. doi:10.1016/j.ceramint.2013.07.016.

[30] S. Cers, Preparation and characterization of CdTe thin films deposited by CSS, **37** (1995) 273–281.

[31] M.S. Islam, J. Kurawaki, Y. Kusumoto, M.Z. Bin Mukhlish, P. Science, V. Science, Hydrothermal Novel Synthesis of Neck-structured Hyperthermia-suitable, (2012). doi:10.3329/jsr.v4i1.8727.

[32] M.J. Prest, Q.T. Zhao, J.T. Muhonen, V.A. Shah, J.S. Richardson-Bullock, M. Prunnila, D. Gunnarsson, T.E. Whall, E.H.C. Parker, D.R. Leadley, Using platinum silicide as a superconductor for silicon electron coolers, ULIS 2013 14th Int. Conf. Ultim. Integr. Silicon, Inc. "Technology Brief. Day." **75** (2013) 201–204. doi:10.1016/j.mssp.2017.12.003.

[33] N. Özer, F. Tepehan, Optical and electrochemical characteristics of sol-gel deposited iron oxide films., Sol. Energy Mater. Sol. Cells. **56** (1998) 141. doi:10.1016/S0927-0248(98)00152-4.

[34] M. Gartner, M. Crisan, A. Jitianu, R. Scurtu, R. Gavrila, I. Oprea, M. Zaharescu, Spectroellipsometric characterization of multilayer sol-gel Fe_2O_3films, J. Sol-Gel Sci.

Technol. **26** (2003) 745–748. doi:10.1023/A:1020706423230.

[35] A.A. Akl, Optical properties of crystalline and non-crystalline iron oxide thin films deposited by spray pyrolysis, Appl. Surf. Sci. **233** (2004) 307–319. doi:10.1016/j.apsusc.2004.03.263.

[36] L. Dghoughi, B. Elidrissi, C. Bernède, M. Addou, M.A. Lamrani, M. Regragui, H. Erguig, Physico-chemical, optical and electrochemical properties of iron oxide thin films prepared by spray pyrolysis, Appl. Surf. Sci. **253** (2006) 1823–1829. doi:10.1016/j.apsusc.2006.03.021.

[37] M. Zhang, W. Luo, Z. Li, T. Yu, Z. Zou, Improved photoelectrochemical responses of Si and Ti codoped α-Fe_2O_3photoanode films, Appl. Phys. Lett. **97** (2010) 4–7. doi:10.1063/1.3470109.

[38] H. Zhang, A. Xie, C. Wang, H. Wang, Y. Shen, X. Tian, Novel rGO/α-Fe_2O_3 composite hydrogel: Synthesis, characterization and high performance of electromagnetic wave absorption, J. Mater. Chem. A. 1 (2013) 8547–8552. doi:10.1039/c3ta11278k.

[39] W. Xiao, Z. Wang, H. Guo, X. Li, J. Wang, S. Huang, L. Gan, Fe_2O_3particles enwrapped by graphene with excellent cyclability and rate capability as anode materials for lithium ion batteries, Appl. Surf. Sci. 266 (2013) 148–154. doi:10.1016/j.apsusc.2012.11.118.

[40] F. Cheng, K. Huang, S. Liu, J. Liu, R. Deng, Surfactant carbonization to synthesize pseudocubic α-Fe_2O_3/C nanocomposite and its electrochemical performance in lithium-ion batteries, Electrochim. Acta. **56** (2011) 5593–5598. doi:10.1016/j.electacta.2011.04.002.

[41] A.M. El Sayed, S. Taha, G. Said, F. Yakuphanoglu, Superlattices and Microstructures Controlling the structural and optical properties of nanostructured ZnO thin films by cadmium content, SUPERLATTICES Microstruct. **65**(2014)35–47. doi:10.1016/j.spmi.2013.10.041.

[42] A.M. El Sayed, W.M. Morsi, S. Mahrous, A. Hassen, Properties of Polyvinyl Chloride / Cadmium Oxide Nanocomposite Films, (2014). doi:10.1002/pc.

[43] M. Sorescu, R.A. Brand, D. Mihaila-Tarabasanu, L. Diamandescu, The crucial role of particle morphology in the magnetic properties of haematite, J. Appl. Phys. **85** (1999) 5546–5548. doi:10.1063/1.369890.

الملخص العربى للبحث

العنوان "تأثير درجة الحراره لمركب أكسيد الحديد النانومترى (α-Fe_2O_3) على التركيب والخواص الضوئية"

تم تصنيع جسيمات أكسيد الحديد النانومترية (α-Fe_2O_3) بإستخدام طريقة التفاعل الصلبه باستخدام كلوريد الحديد($FecL_2$&$FecL_3$) وذالك فى وجود PVP(Polyvinylpyrrolidone) . إستخدام PVP يوفر الأستقرار على المدى الطويل وكذالك منع تكتل جسيمات أكسيد الحديد النانومترية . تم تشكيل جسيمات (α-Fe_2O_3) بواسطة التكوين الحرارى عند درجات حرارة مختلفة (800&200,300,400,500,600,700) درجة مئوية وقد بدأ تكون الجسيمات النانومترية عند درجة حرارة 400 درجة مئويه وعند زيادة درجة الحرارة ذادت درجة التبلور وبدراسة الحصائص التركيبية للجسيمات النانومترية للهيماتيت (الشكل -الحجم- الحالة الكيميائية) بواسطة تقنيات (XRD, UV-vis, SEM, EDAX,VSM)

تم تأكيد الشكل الكروى المتجانس لطبيعة السطح بواسطة التصوير المجهرى للضوء SEM وكان حجم الجسيمات يتراوح بين 30-12 nm.

وتعتبر طريقة تفاعل الحالة الصلبة لتحضير مسحوق α-Fe_2O_3 طريقة بسيطة وغير مكلفة وصديقة للبيئة ويمكن إستخدامها لتحضير حبيبات نانومتريى لمواد أخرى .